Investigations on the slope efficiency of a pulsed 2.8-μm Er^{3+}:$LiYF_4$ laser

M. Pollnau,* R. Spring, S. Wittwer, W. Lüthy, and H. P. Weber

Institute of Applied Physics, University of Bern, Sidlerstrasse 5, CH-3012 Bern, Switzerland

Received October 16, 1996

A slope efficiency of 40% from an Er^{3+}:$LiYF_4$ laser is demonstrated under pulsed Ti:sapphire pumping at 973 nm. With reduction of the pump-pulse duration a significant decrease of the slope efficiency and an increase of the threshold is observed in the experiment and confirmed with high accuracy in a computer simulation. This behavior is due to interionic upconversion from the lower laser level, which leads to energy recycling into the upper laser level. The upconversion rate is negative at threshold but increases strongly with rising pump-pulse energy, thus enhancing the slope efficiency. The conditions are derived that are necessary for achieving the high slope efficiency of the energy-recycling regime. © 1997 Optical Society of America
[S0740-3224(97)03504-2]

1. INTRODUCTION

In recent years there has been an increased interest in lasers emitting at 3 μm mainly because of their potential applications in laser surgery. Owing to the high absorption of 3-μm radiation in water, high-quality cutting or ablation is demonstrated in biological tissue by use of erbium-doped solid-state lasers. With rising temperature the irradiated tissue at the incision site does not show the same absorption coefficient as pure liquid water.[1] Owing to the wavelength shift toward shorter wavelengths,[1] the Er^{3+}:$LiYF_4$ emission at 2.81 μm seems to be possibly better suited for corresponding medical applications than the Er^{3+}:$Y_3Al_5O_{12}$ laser emitting at 2.94 μm.

Surgery with laser radiation brought to the operation site by endoscope, as in orthopedy, is normally performed in aqueous media. Long pulses (pulse duration 400 μs) of 3-μm radiation lead to an optimum in efficiency of tissue ablation[2] when applied in liquid surroundings. These pulses can be generated either by pulsed modulation of the cw output or by pulsed excitation of the laser. However, pulsed excitation of an erbium 3-μm laser affects the efficiency of the laser output. Nevertheless, a high efficiency of the laser output is essential for clinical applications.

Owing to the relatively long lifetime of the $^4I_{11/2}$ upper laser level in $LiYF_4$ of approximately 4 ms,[3] high slope efficiencies can be expected in this material under cw excitation.[4] Slope efficiencies of 35% for a diode-pumped Er^{3+}(15%):$LiYF_4$ laser[5] and 36% for a Ti:sapphire-pumped Er^{3+}(30%):GSGG laser[6] have been reported under cw excitation. In this contribution the dependence of the slope efficiency of an Er^{3+}:$LiYF_4$ laser at 2.81 μm on the pump-pulse duration is investigated. A value of 40% is obtained with 20-ms pulse duration. A decrease of the slope efficiency with shortening of the pump-pulse duration is found experimentally. This behavior is confirmed with high accuracy by a computer simulation. The excitation dynamics of the system are discussed.

2. EXPERIMENT

The experimental arrangement is shown in Fig. 1. An Er^{3+}(15%):$LiYF_4$ laser crystal of length ℓ=4.5 mm is used for our experiments. The dopant concentration of 15 at. % on the Y^{3+} site in $LiYF_4$ was found to be optimal for the 3-μm transition.[5] Commercial antireflection coatings at 3 μm had to be removed from the crystal surfaces before laser emission could be obtained. The crystal is cut plan/plan parallel and is placed in the resonator with the surfaces adjusted perpendicular to the resonator axis.

The erbium ions are excited with an Ar^+-laser-pumped Ti:sapphire laser at λ_p = 973 nm by directly pumping into the $^4I_{11/2}$ upper laser level; see Fig. 2. The 970-nm pump band is more efficient than other pump wavelengths used for this laser transition.[6] The pump beam is linearly polarized parallel to the crystal a axis. The measured atomic cross sections at 973 nm with polarization parallel to the crystal a axis are as follows: ground-state absorption (GSA) cross section[7] $\sigma_{02} = 0.6 \times 10^{-20}$ cm^2 and excited-state absorption (ESA) cross section $\sigma_{26} = 0.8 \times 10^{-20}$ cm^2 (calculated from the ESA spectrum of Ref. 7 under consideration of the relative population factor of 60%). Since ground-state bleaching and hence ESA are small, the resulting absorption coefficient is approximately 12.4 cm^{-1} at 15% dopant concentration. More than 99% of the pump power is absorbed within the crystal.

The TEM_{00} mode structure of the pump beam is controlled with a CCD camera. The pump beam is chopped with a frequency of 16.7 Hz and a duty cycle of 33%, which provides an excitation time of 20 ms. Therefore the laser operates practically in the cw regime when the excitation time is compared with the effective lifetimes (including interionic processes) of the laser levels of the order of approximately 1 ms (see Ref. 4 and later in Fig. 6 of this paper). The time between two subsequent pump pulses ensures the complete relaxation of the system. The pump beam is focused onto the crystal front surface with a lens of focal length f = 65 mm. The pump-waist

0740-3224/97/040974-05$10.00

radius at the crystal front surface is approximately $\omega = 40\ \mu$m.

The $LiYF_4$ crystal is mounted on a water-cooled copper block and is placed close to the input mirror of a nearly hemiconcentric resonator of optical length $\ell_{opt} = 75$ mm. Both mirrors, the plane input and the concave (75-mm radius) output mirror, have a nonoptimized reflectivity of $Rf_1 = Rf_2 = 98.8\%$ at the laser wavelength $\lambda_l = 2.81\ \mu$m. The output beam is linearly polarized parallel to the crystal c axis. The laser radiation is measured to be emitted in equal parts on both sides of the resonator. The output power as a function of the pump power launched into the crystal is shown in Fig. 3. A slope efficiency of 40% is obtained. The slope efficiency exceeds the Stokes limit of $\eta_{st} = \lambda_p/\lambda_l = 35\%$. This results from energy recycling into the upper laser level by interionic upconversion W_{11} from the lower laser level;[3,4,6] see Fig. 2. The laser threshold is measured to be 13 mW.

The performance of the laser close to threshold usually exhibits a nonlinear behavior; see Fig. 3. Thus the output characteristics in the linear range at higher pump power, which is of interest for surgical applications, is not sufficiently described by the threshold and the slope efficiency of the laser. Therefore we introduce here a new

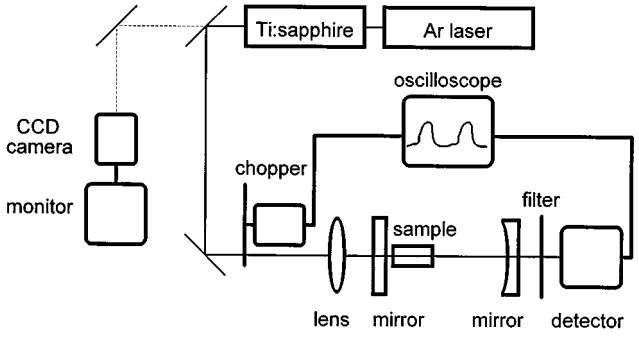

Fig. 1. Experimental arrangement.

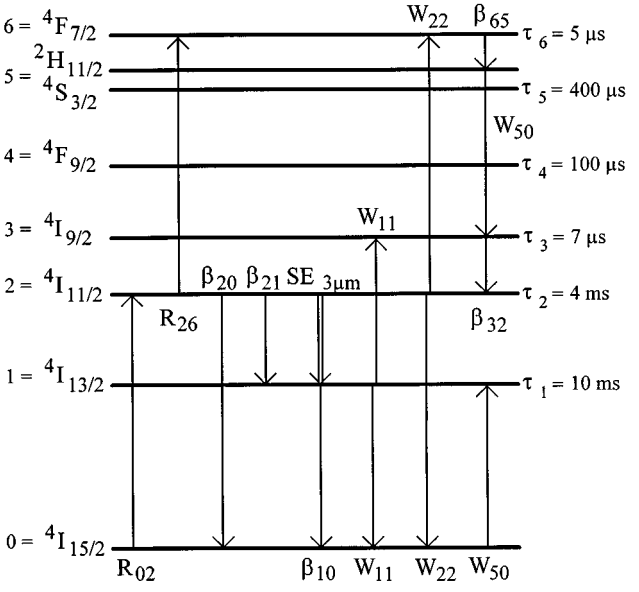

Fig. 2. Energy-level scheme of Er^{3+}:$LiYF_4$, indicating the important excitation mechanisms of the system.

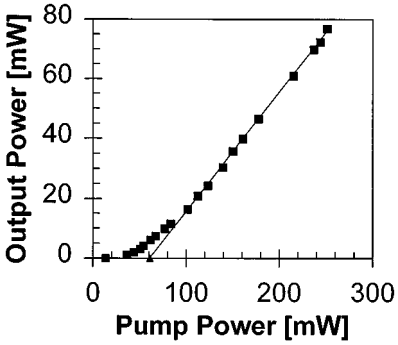

Fig. 3. Output versus input power of an Er^{3+}:$LiYF_4$ laser under Ti:sapphire-laser excitation (20-ms pump pulses). A maximum slope efficiency of 40% is experimentally demonstrated. The threshold of the laser is 13 mW. The slope threshold is 60 mW (triangle).

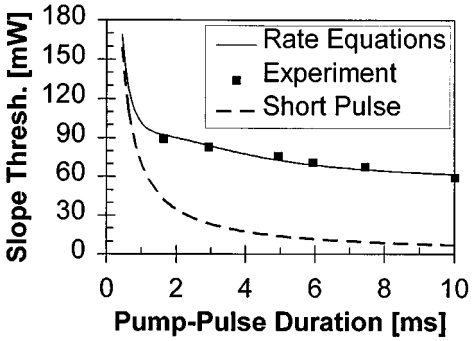

Fig. 4. Slope threshold as a function of the pump-pulse duration. The slope threshold is defined as the zero point of the progression line of the linear input–output slope (cf. triangle in Fig. 3). Data obtained in the experiment and from the computer simulation are compared. The dashed curve indicates the behavior if the pump-pulse duration were short compared with the relevant relaxation-time constants. Data are valid for a pump-beam radius of 40 μm.

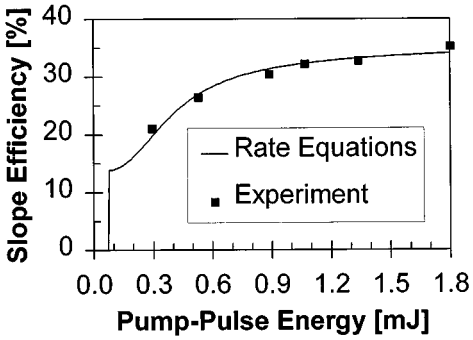

Fig. 5. Slope efficiency as a function of the pump-pulse energy (experimental data: 1.8 mJ = 180-mW input power × 10-ms pump-pulse duration). Data obtained in the experiment and from the computer simulation are compared. Data are valid for a pump-beam radius of 40 μm.

parameter that we call the slope threshold $P_{slope,thr}$. It is defined as the zero point of the progression line of the linear input–output slope. In the present experiment it is determined to be 60 mW (triangle in Fig. 3). The introduction of the slope threshold has practical reasons. One can easily determine this parameter in the experiment as

well as in the computer simulation of Section 3 by measuring or calculating two points in the linear range of the input–output curve and extrapolating to zero-watt output power, whereas for the determination of the real threshold a lot more points have to be calculated in the simulation.

A second experiment is performed with the same experimental arrangement of Fig. 1. However, in the second experiment (a few weeks after the first experiment) the resonator mirrors show a visible degradation of the coatings, probably owing to water contamination. The obtained slope efficiency, therefore, does not exceed 36%. In this experiment the dependence of both slope threshold and slope efficiency on pump-pulse duration is investigated (cf. Figs. 4 and 5). The pump-pulse duration is reduced stepwise from 10 ms to 1.68 ms by varying the duty cycle of the chopper between 33% and 5.6% at a fixed frequency of 33.3 Hz. The output power is measured for input powers of 160, 178, and 198 mW. This procedure is repeated three times in order to decrease the statistical deviation of the data, and the slope efficiency and the slope threshold are determined from the obtained values as a function of the pump-pulse duration at an input power of approximately $P_{\mathrm{in}} = 180$ mW.

The experimental results (squares in Figs. 4 and 5) demonstrate the influence of the pump-pulse duration on slope threshold and slope efficiency. With the reduction of the pump-pulse duration from 10 ms to 1.68 ms (corresponding to a decrease of the pump-pulse energy from 1.8 mJ to 0.3 μJ in Fig. 5) an increase of the slope threshold from 60 mW to 90 mW (Fig. 4) and a decrease of the slope efficiency from 36% to 21% (Fig. 5) is measured.

3. COMPUTER SIMULATION

With the help of a computer simulation that considers all relevant processes (ground state and six excited states; see Fig. 2; GSA, ESA, ground-state depletion, all lifetimes and branching ratios, three interionic processes and their inverse processes, stimulated emission, and the experimental data of crystal and resonator), time-dependent rate equations describing the Er^{3+}:$LiYF_4$ system are solved, the behavior found experimentally is reproduced numerically, and the population dynamics that lead to this behavior are investigated.

The following data are included in the simulation. The Er^{3+}:$LiYF_4$ lifetimes τ_i given in Fig. 2 are data published for 1% erbium concentration[3,8–11] or are mean values of the published data. They represent the intrinsic lifetimes of the system at low dopant concentration and include radiative as well as multiphonon relaxations. The $^4S_{3/2}$ and $^2H_{11/2}$ levels are thermally coupled and are treated as a combined level in the same way as in Ref. 4. The lifetime of the $^4F_{7/2}$ level is assumed. The branching ratios β_{ij} are given in Ref. 4. The parameters of the interionic upconversion processes W_{11} and W_{22} are taken from Ref. 3. The parameters of their inverse processes as well as the parameter of the cross relaxation W_{50} and its inverse parameter are determined from the considerations discussed in Ref. 12. The values used in the present simulation are summarized in Table 1.

Table 1. Parameters of the Interionic Processes and Their Inverse Processes Used in the Simulation

Parameter(10^{-16} cm^3 s^{-1})	Normal Process	Inverse Process
$^4I_{13/2}, {}^4I_{13/2} \rightarrow {}^4I_{9/2}, {}^4I_{15/2}$	$W_{11} = 0.3$	$W_{30} = 0.12$
$^4I_{11/2}, {}^4I_{11/2} \rightarrow {}^4F_{7/2}, {}^4I_{15/2}$	$W_{22} = 0.18$	$W_{60} = 0.18$
$^2H_{11/2}, {}^4I_{15/2} \rightarrow {}^4I_{9/2}, {}^4I_{13/2}$	$W_{50} = 2$	$W_{13} = 2$

The experimental data for the crystal and the resonator parameters of Section 2 are included in the calculation. The radiatively emitted fraction of the rate from upper to lower laser level is $\gamma = 0.29$. The geometrical fraction of the spontaneous emission coupled into the laser mode is $P = 10^{-7}$. The Boltzmann factors of upper and lower Stark laser levels are $b_2 = 0.200$ and $b_1 = 0.113$, respectively.[4] Their degeneracies are $g_2 = g_1 = 2$.

For the simulation, cylindrical and radially homogeneous profiles of pump and laser mode are assumed. The laser-beam radius in the nearly hemiconcentric resonator is slightly larger than the pump-beam radius. A mode overlap of $\eta = 95\%$ between pump and laser mode is assumed that represents the experimental situation. h and c denote Planck's constant and the vacuum speed of light, respectively.

The resonator round-trip loss L is unknown. Experimental values of the atomic emission cross section σ_{21} usually have a large error margin (cf. the discussion in Ref. 13). These two parameters are fitted to reproduce the experimental values for slope threshold and slope efficiency at 10-ms pump-pulse duration (Figs. 4 and 5). Obtained values are $L = 0.7\%$ and $\sigma_{21} = 1.3 \times 10^{-20}$ cm^2. The temporal behavior toward shorter pump-pulse duration then follows automatically from the simulation without the fit of a further parameter. With the above considerations the rate equations for the population densities N_i and the photon density ϕ read

$$\mathrm{d}N_6/\mathrm{d}t = R_{26} - \tau_6^{-1}N_6 + W_{22}N_2^2 - W_{60}N_6N_0, \tag{1}$$

$$\mathrm{d}N_5/\mathrm{d}t = -\tau_5^{-1}N_5 + \beta_{65}\tau_6^{-1}N_6 - W_{50}N_5N_0 + W_{13}N_1N_3, \tag{2}$$

$$\mathrm{d}N_4/\mathrm{d}t = -\tau_4^{-1}N_4 + \sum_{i=5\ldots6}(\beta_{i4}\tau_i^{-1}N_i), \tag{3}$$

$$\mathrm{d}N_3/\mathrm{d}t = -\tau_3^{-1}N_3 + \sum_{i=4\ldots6}(\beta_{i3}\tau_i^{-1}N_i) + W_{50}N_5N_0 - W_{13}N_1N_3 + W_{11}N_1^2 - W_{30}N_3N_0, \tag{4}$$

$$\mathrm{d}N_2/\mathrm{d}t = R_{02} - R_{26} - \tau_2^{-1}N_2 + \sum_{i=3\ldots6}(\beta_{i2}\tau_i^{-1}N_i) - 2W_{22}N_2^2 + 2W_{60}N_6N_0 - R_{\mathrm{SE}}, \tag{5}$$

$$\mathrm{d}N_1/\mathrm{d}t = -\tau_1^{-1}N_1 + \sum_{i=2\ldots6}(\beta_{i1}\tau_i^{-1}N_i) + W_{50}N_5N_0 - W_{13}N_1N_3 - 2W_{11}N_1^2 + 2W_{30}N_3N_0 + R_{\mathrm{SE}}, \tag{6}$$

$$dN_0/dt = -R_{02} + \sum_{i=1..6} (\beta_{i0}\tau_i^{-1}N_i) - W_{50}N_5N_0 + W_{13}N_1N_3 + W_{11}N_1^2 - W_{30}N_3N_0 + W_{22}N_2^2 - W_{60}N_6N_0, \quad (7)$$

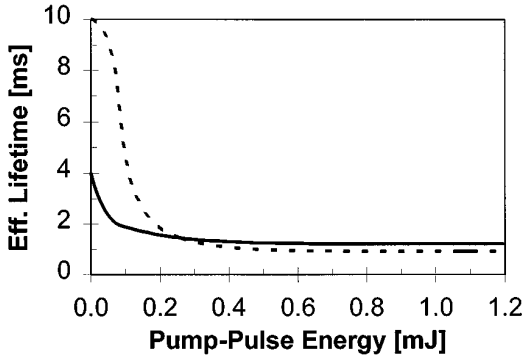

Fig. 6. Effective lifetimes of upper laser level (solid curve) and lower laser level (dashed curve) versus pump-pulse energy. These values include the depletion rates of radiative and multiphonon decay as well as interionic upconversion, as discussed in the text. Data are valid for a pump-beam radius of 40 μm.

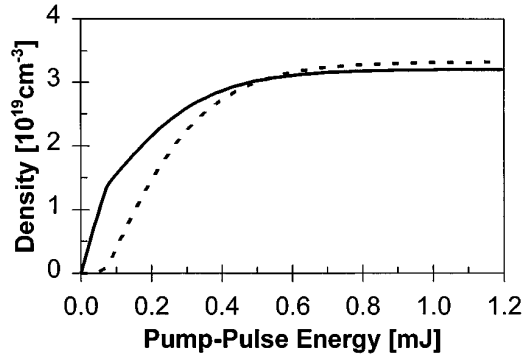

Fig. 7. Population densities of the $^4I_{11/2}$ upper laser level (solid curve) and the $^4I_{13/2}$ lower laser level (dashed curve) versus pump-pulse energy. Data are valid for a pump-beam radius of 40 μm.

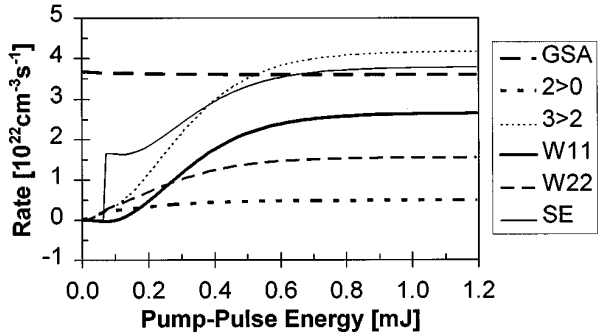

Fig. 8. Important transition rates versus pump-pulse energy. The rates of the processes denoted with W_{11} and W_{22} are the sums of normal and inverse upconversion processes. The following processes that have significant rates are not shown in the figure: The multiphonon rate $^4F_{7/2} \rightarrow {}^2H_{11/2}/{}^4S_{3/2}$ and the cross-relaxation rate W_{50} are comparable to the rate W_{22}. The transition rates $^4I_{11/2} \rightarrow {}^4I_{13/2}$ and $^4I_{13/2} \rightarrow {}^4I_{15/2}$ are smaller than the rate $^4I_{11/2} \rightarrow {}^4I_{15/2}$, which is denoted by $2 > 0$. The ESA rate at the pump-pulse energy of 1.2 mJ is only approximately 2% of the GSA rate. Data are valid for a pump-beam radius of 40 μm.

$$d\phi/dt = (\ell/\ell_{opt})(P\gamma\beta_{21}\tau_2^{-1}N_2 + R_{SE}) + \ln[(1-L)Rf_1Rf_2]c\phi/(2\ell_{opt}). \quad (8)$$

The stimulated-emission rate R_{SE} is given by

$$R_{SE} = [b_2N_2 - (g_2/g_1)b_1N_1]\sigma_{21}c\phi. \quad (9)$$

The equation for the pump rate R_{ij} from level i into level j reads

$$R_{ij} = \frac{\sigma_{ij}N_i}{\sigma_{02}N_{02} + \sigma_{26}N_{26}}\{1 - \exp[(\sigma_{02}N_0 + \sigma_{26}N_2)\ell]\}\lambda_p/(hc\ell\pi\omega^2)\eta P_{in}. \quad (10)$$

Equation (10) considers ground-state depletion and population of an ESA level dynamically. The output power P_{out} is calculated from the equation

$$P_{out} = 0.5c\phi(hc/\lambda_l)\pi\omega^2(1 - Rf_1Rf_2). \quad (11)$$

The rate equations are solved time dependently, but without longitudinal or radial resolution of the active medium, in a Runge–Kutta calculation of fourth order. The relaxation oscillations that occur when the laser reaches threshold are suppressed in the simulation in order to obtain nonoscillating values for slope efficiency and slope threshold also in the region of the oscillations. Results are given in Figs. 4–8.

4. DISCUSSION

The results of the computer simulation are in excellent agreement with the measured data; cf. Figs. 4 and 5. From the simulation, values of the effective lifetimes (Fig. 6), the population densities of the excited levels (Fig. 7), and the transition rates of the involved processes (Fig. 8) are obtained. This provides a deeper insight into the population mechanisms of the system.

Laser emission has a slope-threshold energy of 70 μJ; see Fig. 5. If the pump-pulse duration were short compared with the important relaxation-time constants of the system, the product of slope-threshold power times pump-pulse duration would be constant (=70 μJ) and the slope-threshold power would exhibit a hyperbolic behavior versus pump-pulse duration, as indicated in Fig. 4 (dashed curve). However, as the intrinsic lifetimes of the laser levels are strongly quenched by interionic upconversion processes and the resulting effective lifetimes are of the order of 1 ms (see Fig. 6), the behavior of the system already deviates from the hyperbolic curve in the range of 1-ms pump-pulse duration; see Fig. 4. In the quasi-cw regime at 10-ms pump-pulse duration it reaches a slope-threshold power of 60 mW; cf Figs. 4 and 3.

The calculation of the effective lifetimes of Fig. 6 requires a comment. The values are derived from the equation

$$1/\tau_{eff} = 1/\tau_i + W_{ii}N_i, \quad (12)$$

which takes into account the depletion of level i by its intrinsic rate as well as the removal of one excitation by each upconversion process. Originally, each upconversion process removes two excitations from level i; cf. the corresponding terms in Eqs. (5) and (6). The excitation upconverted by the process W_{22}, however, is efficiently recycled by the cross relaxation W_{50} and the subsequent

multiphonon relaxation (see Fig. 2), whereas the excitation upconverted by the process W_{11} is recycled by the same multiphonon relaxation and the subsequent laser process. Thus if the effective lifetime is calculated versus initial pump energy, only approximately one excitation is removed from the originating level. Another approach that would lead to the same result consists of multiplying the upconversion rate in Eq. (12) by a factor of two and simultaneously considering the additional pump excitation of the laser levels evoked by the processes mentioned above.

The slope efficiency (Fig. 5) in the first temporal part of laser emission is 14% but rapidly increases with rising pump energy until it reaches a saturation level in the range of the Stokes limit of 35% above a pump-pulse energy of 1 mJ. The reason for this behavior is determined with the knowledge of the population densities of the laser levels (Fig. 7) and the important transition rates of the system (Fig. 8).

In the first temporal part the upper laser level is populated solely by direct pump excitation. At threshold the upconversion rate W_{22} from this level and subsequent cross relaxation W_{50} are already significant. Excitation is transferred by these processes to the $^4I_{9/2}$ level. Beside multiphonon relaxation into the upper laser level, a small cross-relaxation rate involving the $^4I_{9/2}$ level and the ground state is present that is larger than the upconversion rate from the practically unpopulated lower laser level. Consequently, the summed rate of normal and inverse processes, upconversion from and cross relaxation into the lower laser level, is negative at threshold.

With rising pump excitation and laser emission the population of the lower laser level increases (Fig. 7), and energy recycling by upconversion from lower to upper laser level becomes relevant. The recycled energy (with its rate given by W_{11} in Fig. 8) increases the slope efficiency of the system because it represents an additional feeding of the upper laser level. At 10-ms pump-pulse duration, the upconversion rate $^4I_{13/2} \rightarrow {}^4I_{9/2}$ and the relaxation rate $^4I_{13/2} \rightarrow {}^4I_{15/2}$ from the lower laser level (including their inverse processes) are approximately 8 times stronger than the linear relaxation rate. This means that almost half of the excitation of the lower laser level is recycled into the upper laser level.

This significant change in the input–output dynamics of the system after the laser threshold is reached is due to the quasi-four-level nature of the erbium 3-μm laser system. The term quasi four level expresses the fact that the lifetime of the lower laser level has a significant value. This means that the population densities of the laser levels are not clamped at their threshold values, but additional pumping further increases the excitation of both laser levels.

The cw excitation density of the whole system, which is equivalent to the amount of ground-state bleaching, is 3% for the given pump parameters. This excitation is mostly accumulated in equal parts in the laser levels; see Fig. 7. Thus ESA from the upper laser level, which has an absorption cross section comparable to that of GSA (cf. Section 2), has no influence because the resulting ESA coefficient reaches only 2% of the GSA coefficient at cw excitation.

The result of our computer simulation is similar to that obtained by analytical rate-equation solutions for Er^{3+} in $Y_3Al_5O_{12}$.[14] In order to achieve a high slope efficiency >30% in $LiYF_4$ with pump-pulse durations of the order of 400 μs, which are desirable for surgical applications, the pump-pulse energy should exceed a value of 1 mJ for a given pump focus of 40-μm radius.

5. CONCLUSIONS

A slope efficiency of 40% from an Er^{3+}(15%):$LiYF_4$ 2.8-μm laser is demonstrated. This value exceeds the Stokes limit of 35% owing to energy recycling from lower to upper laser level. Under pulsed excitation a significant increase of the slope efficiency from 14% to 36% and a decrease of the slope threshold with rising pump-pulse energy is experimentally observed and reproduced with high accuracy by a computer simulation. Energy recycling by interionic upconversion from lower to upper laser level is responsible for this behavior. A slope efficiency exceeding 30% can only be reached by the equivalent of a pump-pulse energy of 1 mJ focused to a radius of 40 μm at 400-μs pump-pulse duration. This can be considered as the lower limit for an efficient 3-μm Er^{3+}:$LiYF_4$ laser for surgical applications.

ACKNOWLEDGMENT

This work was supported in part by the Swiss Priority Program Optique.

*Present address: Optoelectronics Research Centre, University of Southampton, Southampton SO17 1BJ, UK.

REFERENCES

1. S. L. Jacques and G. Gofstein, *Laser–Tissue Interaction II*, S. L. Jacques, ed., Proc. SPIE **1427**, 63 (1991).
2. M. Ith, H. Pratisto, H. J. Altermatt, M. Frenz, and H. P. Weber, Appl. Phys. B **59**, 621 (1994).
3. H. Chou and H. P. Jenssen, in *Tunable Solid State Lasers*, M. L. Shand and H. P. Jenssen, eds., Vol. 5 of OSA Proceeding Series (Optical Society of America, Washington, D.C., 1989), p. 167.
4. M. Pollnau, Th. Graf, J. E. Balmer, W. Lüthy, and H. P. Weber, Phys. Rev. A **49**, 3990 (1994).
5. T. Jensen, A. Diening, G. Huber, and B. H. T. Chai, Opt. Lett. **21**, 585 (1996).
6. R. C. Stoneman and L. Esterowitz, Opt. Lett. **17**, 816 (1992).
7. M. Pollnau, W. Lüthy, H. P. Weber, K. Krämer, H. U. Güdel, and R. A. McFarlane, Appl. Phys. B **62**, 339 (1996).
8. J. Rubin, A. Brenier, R. Moncorgé, and C. Pedrini, J. Lumin. **36**, 39 (1986).
9. D. S. Knowles and H. P. Jenssen, IEEE J. Quantum Electron. **28**, 1197 (1992).
10. R. Brede, T. Danger, E. Heumann, G. Huber, and B. H. T. Chai, Appl. Phys. Lett. **63**, 729 (1993).
11. C. Li, Y. Guyot, C. Linarès, R. Moncorgé, and M. F. Joubert, in *Advanced Solid-State Lasers and Compact Blue-Green Lasers*, Vol. 2 of 1993 OSA Technical Digest Series (Optical Society of America, Washington, D.C., 1993), p. 423.
12. M. Pollnau, W. Lüthy, and H. P. Weber, J. Appl. Phys. **77**, 6128 (1995).
13. J. Koetke and G. Huber, Appl. Phys. B **61**, 151 (1995).
14. A. M. Prokhorov, V. I. Zhekov, T. M. Murina, and N. N. Platnov, Laser Phys. **3**, 79 (1993).